Investigation of Volume of Fluids (VOF) Method and System Models for Design of Microfluidic Ink Delivery Apparatus for Dip Pen Nanolithography (DPN)

D. Banerjee*

*Mechanical Engineering, Texas A&M University,
3123 TAMU, College Station, TX 77843-3123, USA.

ABSTRACT

DPN™ is a versatile technology that leverages Scanning Probe Microscopy for applications in biotechnology, photomask repair, molecular-electronics, nano-electronics and mask-less lithography. The DPN process was augmented for biotechnology applications (genomics, proteomics) through the design, development, prototype fabrication, testing and manufacture of commercial microfluidic systems called "Inkwells™". In this study VOF method was used to simulate and optimize the design of micro-capillary flows in Inkwells. Subsequently the simulations were verified experimentally. Based on these results a novel system model was developed to predict the temporal sequence of flow in the different parts of the microfluidic network.

Keywords: lab-on-chip, micro-capillary flow, meniscus bifurcation, bubble trap

1 INTRODUCTION

The Dip Pen Nanolithography™ (or "DPN™") process uses scanning probe tips (the "pen") coated with chemicals ("ink") to directly deposit materials with nanometer precision onto a substrate ("paper")[1]. Under ambient conditions, the DPN process can deposit a variety of inorganic, organic and biological molecules onto a variety of substrate types[2]. When using oligomer or protein-based inks, DPN method can produce nanoscale spotted features which are much smaller than those observed in bio-arrays[3] fabricated by other methods. DPN™ is a versatile technology that leverages Scanning Probe Microscopy for applications in biotechnology, photomask repair, molecular-electronics, nano-electronics and mask-less lithography [1].

To enable parallel writing of multiple patterns using the DPN process an NSCRIPTOR™ system integrated with an array of pens was developed to simultaneously write multiple patterns with different inks. This requires selective deposition (i.e., coating) of ink chemistries onto the individual pens. This is accomplished by "dipping" the multi-pen array into an array of microwells formed in the "Inkwells™." The various components of the "Inkwells" microfluidic system consisted of: reservoirs, microchannel networks with main artery and tributaries, satellite reservoirs and dispensing micro-wells. The device was designed to deliver between 4 aqueous inks (for genomics applications) and 10 aqueous inks (for proteomics applications) into appropriately spaced microwell array. Fluid actuation occurs by open-channel capillary flow (wicking) in microchannels, which distribute liquid from reservoirs into a microchannel reservoir and ultimately to an array of terminal microwells connected by tributaries from the microchannel (Fig. 1). The end of the tributary microchannels communicates with a set of microwells which range from 5 to 10 microns in diameter. Satellite reservoirs are incorporated in some of the layouts to serve as secondary sites of liquid storage and also for trapping bubbles in the flow.

In this study VOF simulations were performed for both open channel and pipe flow configurations of the microfluidic system. The VOF method was optimized for simulating micro-capillary pumping in the microfluidic networks. The fluidic process for meniscus bifurcation in open-channel flows and pipe flows were studied to understand the mechanics of bubble formation for micro-capillary flows in distributed network of microchannels. The VOF simulations were used to develop system models for predicting microcapillary filling in Inkwells.

2 ANALYSIS

The flow rates in the microchannels were calculated from a balance of the capillary and viscous forces (and neglecting inertial forces):

$$\Delta p_m = \frac{4\sigma Cos\theta}{D_{hm}} = \frac{1}{2}\rho u^2 f \frac{L}{D_{hm}} \quad (1)$$

where, p: is pressure drop, σ is the coefficient of surface tension, θ is the contact angle, D_h is the hydraulic diameter of the channel (where $D_{hm} = 4A/P_w$, A is the cross sectional area for flow direction; P_w is the wetted perimeter of the cross section), ρ is the density of liquid flowing in the microchannels, u is the average velocity in the microchannels, f is the Darcy-Weisbach friction factor [4, 5], L is the length of the channel. For laminar flow in circular channels, $f = 64/Re_{Dh}$, where $Re_{Dh} = \rho\, u\, D_h / \mu$, where Re_{Dh} is the Reynolds number and μ is the kinematic viscosity of the working liquid. For rectangular channels, the friction coefficient is within -11% to +40% of the value for circular channels, depending on the aspect ratio, where aspect ratio = height/width. For example, for a rectangular channel of aspect ratio 10, the friction factor is given by f =

$84.68/Re_{Dh}$, which is 30% higher than for a circular cross section. For a square cross section (aspect ratio = 1), the friction factor is given by $f = 56.91/Re_{Dh}$, which is 11% lower than for a circular cross section. Other values of friction factor can be obtained for different aspect ratios in many standard introductory text books on thermo-fluidics [4, 5].

Using the formulation for f (valid for $Re_{Dh} < 2000$) for a generalized cross section, Equation (1) can be simplified as:

$$uL = D_h \sigma Cos\theta / 8\mu \quad (2)$$

Using properties of water, the initial velocity of fluid flow in the microchannels can be calculated to be of the order of 1m/s for $L/D_h > 10$. This estimate matched very well with experimental data described later. Equation (2) can be used to estimate the filling time (τ_{12}) as:

$$\tau_{12} = \int_{L_1}^{L_2} \partial L/u = \frac{1}{2}\left(L_2^2 - L_1^2\right)\frac{8\mu}{D_h \sigma Cos\theta} \quad (3)$$

Equation (3) can be written in non-dimensional form as:

$$\left[\frac{\sigma Cos\theta / D_h}{4\mu}\right]\tau_{12} = \frac{L_2^2 - L_1^2}{D_h^2} \quad (4)$$

Equation (3) is used to calculate filling time of microchannels of different hydraulic diameters using the following thermo-physical properties: $\mu = 10^{-5}$ kg /m-s, $\sigma =$ 0.07 N/m, and $\theta = 20°$. The results of the calculation are plotted in Fig. 2. The results show that for the same length the wider channels (larger D_h) fill up faster than the narrow channels. This is due to capillary forces ($\sim 1/D_h$) being retarded by even larger pressure drop ($\sim D_h^2$) in narrow microchannels. The analysis also shows that open-channel flow has smaller filling time (lower D_h) than for pipe flow.

3 NUMERICAL MODEL

Volume of Fluids (VOF) method was used to verify the analysis mentioned above. Also, a design choice to use closed-channel flow (or "pipe flow") or open-channel flow was made based on the CFD simulation results. The models were created and tested using the VOF method in the CFD-ACE+ design and simulation multi-physics software (ESI Corporation, Hunstville, AL). In open-channel flow, there is less susceptibility to bubble formation for liquid flow in the microchannels and during the filling of the microwells. However, the trade off for this design is the enhanced evaporative loss of the inks, especially for liquids with high vapor pressure under ambient conditions. The evaporative losses in closed-channel (or pipe flow) are lower - however, the microwells, microchannels and reservoirs have a greater propensity to form bubbles during filling. Bubble formation in these components can impede capillary flow and can lead to catastrophic failure for fluid actuation in these devices. It was verified from the simulations that the filling time is lower in open-channel than pipe flow and is consistent with the analytical results. Figs. 3 and 4 show a simulation of meniscus break-up from a 5µm wide channel into a 2µm wide tributary (both 10µm deep) using the Volume of Fluids (VOF) method. The simulations were performed for thermo-fluidic property values of water at room temperature (where T = 298 K, $\rho = 996.5$ kg/m^3, $\mu = 10^{-3}$ kg/m-s, $\sigma = 0.07$ N/m, $\theta = 20°$). For pipe flow simulations, the boundary conditions imposed were: wall boundary conditions on the sides, outlet boundary condition at the end of the channels and inlet boundary condition at the beginning of the channel flow region. For open-channel flow simulations, the boundary conditions imposed were: wall boundary conditions on the sides, outlet boundary condition at the end of the channels, outlet boundary conditions on the top surface and inlet boundary condition at the beginning of the channel flow region. For both set of simulations, a fluid initial condition was imposed with a stationary volume of liquid, which was 40 microns long from the inlet region.

The sequence of images in Fig. 3 shows that the meniscus break-up process is initiated at the top and bottom wall in pipe flow. The images in Fig. 4 show that the meniscus break-up process is initiated at the bottom wall for open-channel flow and therefore has less susceptibility to trap bubbles during the filling process. The simulation data also validate the analytical prediction that the filling is process is faster in the wider channel compared to the narrower tributary channel. By measuring the time of travel of the meniscus in the wider microchannel (before meniscus bifurcation and flow distribution into the smaller tributary microchannels) – the speed of the meniscus movement was found to be of the order of 1m/s. This is consistent with results from Equation 3 for $L/D_h > 10$ and using the thermo-physical property values of water mentioned above. The numerical results showed that there is a reduction in the velocity of the meniscus when the flow is distributed from the wider microchannel into the tributaries. This is expected due to higher pressure drop that occurs on distribution of the flow into more than one microchannel compared to the enhanced capillary pressure arising from bifurcation of menisci.

4 SYSTEM MODEL

The VOF simulations required high mesh integrity for reasonable solver accuracy and the individual simulations required 1-3 weeks to complete. To obviate long simulation times typically encountered in Computational Fluid Dynamic models while maintaining reasonable accuracy – behavioral system models are typically used (also known as "Macro-Model", "Spice" or "T-Spice Model", "Reduced Order Model" or "Lumped Parameter Model"). The system model was based on the principle of electrical networks (Kirchoff's Law) and the

concept of R-L-C (Resistance-Inductance-Capacitance) device models applied to microfluidic devices (Fig. 5).

Fig. 6 shows the equivalent system model for a microfluidic network distributing flow into tributaries. Here a time dependent flow resistance is used to model the flow into tributaries. Any leg i of the microchannel consists of two sets of resistors, $R_{i-1,\ i}$ (main channel) and R_{Ti} (tributary), capillary pressures ΔP_m (Eq. 1) and ΔP_{Ti} (where D_{Th} of tributary capillary channel is substituted in Eq. 1), and flow velocities u_i and u_{Ti} (tributary). Based on these parameters, the governing equations are written as:

$$(\Delta p_m) = \sum_{i=1}^{n} R_i u_i f(t - \tau_{i-1,i}) \quad (5)$$

$$(\Delta p_T) = \sum_{i=1}^{n} R_{Ti} u_{Ti} f(t - \tau_{i-1,i}) f(\tau_{Ti} - t) \quad (6)$$

$$\sum_{i=1}^{n} u_i f(t - \tau_{i-1,i}) = \sum_{i=1}^{n} u_{Ti} f(t - \tau_{i-1,i}) f(\tau_{Ti} - t) \quad (7)$$

where τ_{Ti} is obtained from Eq. 4 after substituting the values for the tributary microchannel, and the flow resistance values are given by:

$$R_i = \frac{128\mu}{D_{mh}^4} \sqrt{\frac{D_{mh}\sigma\cos\theta\tau_{i-1,i}}{8\mu} + \sum_{i=1}^{n} (L_i f(t - \tau_{i-1,i})^2} \quad (8)$$

$$R_{Ti} = \frac{128\mu}{D_{Th}^4} \sqrt{\frac{D_{Th}\sigma\cos\theta\tau_{Ti}}{8\mu} + [\sum_{i=1}^{n} L_i f(t - \tau_{i-1,i}) f(t - \tau_{Ti})]^2} \quad (9)$$

and the time control function, f is given by:

$$f(t - \tau) = 1 \text{ for } (t - \tau) > 0;$$
$$= 0 \text{ for } (t - \tau) < 0$$

The linear set of equations given by Eq. 5, 6 and 7 are solved at a given time t for the unknown values of u_i and u_{Ti} by substituting the time-dependent flow resistance values from Eq. 8 and 9.

5 CONCLUSION

Analytical, numerical and system models have been derived in this study for modeling flow in Inkwells. The analytical models were validated by simulations from numerical models and it was found that open channel flow fills faster and has fewer propensities for forming bubbles.

REFERENCES

[1] Piner, C. A., *et al.*, 1999, "Dip-Pen Nanolithography", *Science* **283**, 661-663.

[2] Banerjee, D., et al., "Planar capillary pumped ink delivery apparatus for DPN", *Proceedings of the 7th International Conference on Micro Total Analysis Systems (mTAS 2003),* October 5-9, Squaw Valley, CA.

[3] A.D. Barone, *et al.*, "Photolithographic synthesis of high-density oligonucleotide probe arrays", *Nucleosides, Nucleotides & Nucleic Acids*, **20** (4-7), p.525-31, 2001.

[4] F.M. White, *Fluid Mechanics*, 1994, Third Edition, McGraw-Hill Inc.

[5] A.F. Mills, *Heat and Mass Transfer*, 1995, Irwin Inc.

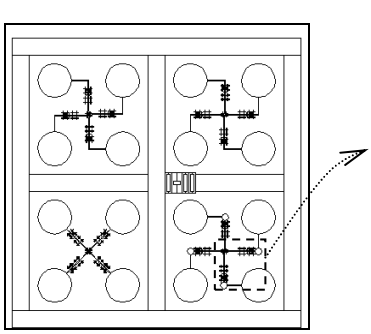

Figure 1. Mask layout showing layouts for delivery of 4 different inks. The inset shows the location of reservoirs (diameter: 1mm), satellite reservoirs, microchannel, alignment marks, microwells and tributaries connecting the microchannels. The microwells are located at the end of the tributaries and are not clearly visible due to the large range of length scales in the layout.

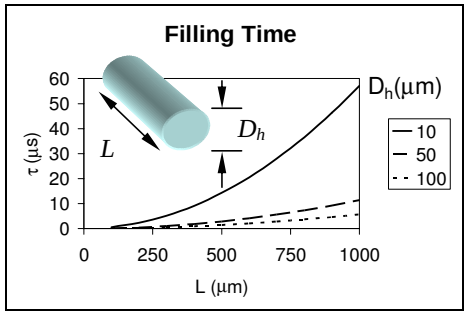

Figure 2. Filling time (τ) in for capillary filling of microchannels of length (L) and hydraulic diameter (D_h) for water.

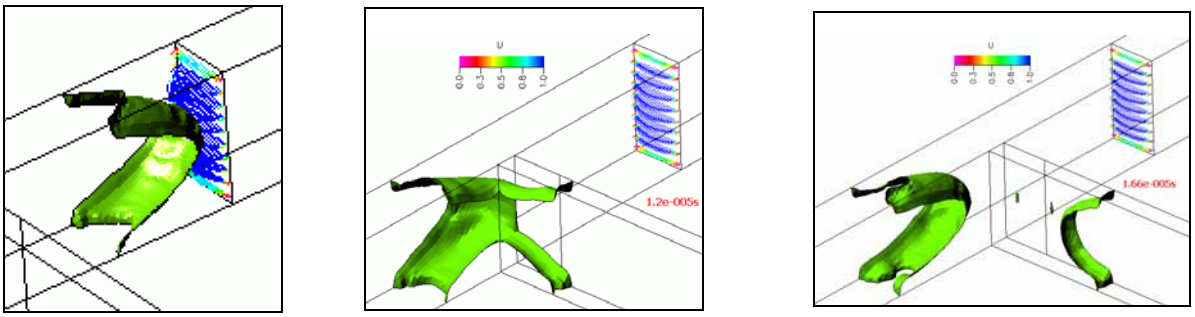

Figure 3. Temporal simulation of meniscus shapes for microchannel filling in pipe flow.

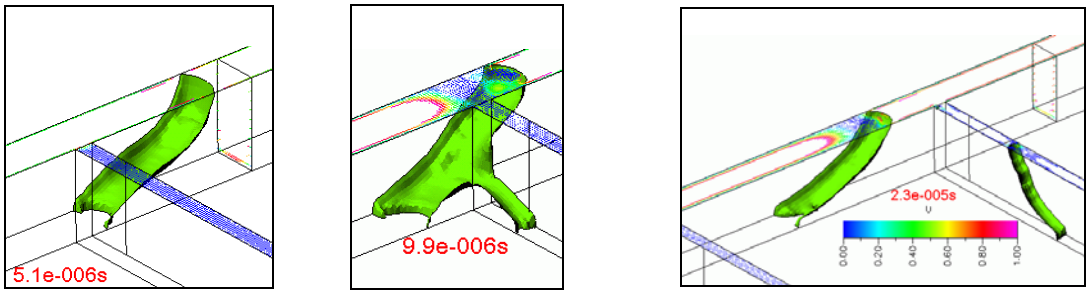

Figure 4. Temporal simulation of meniscus shapes for filling in open-channel flow.

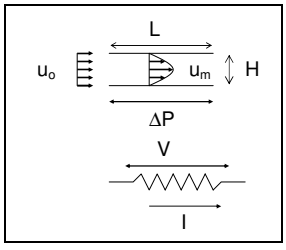

Figure 5. Concept of system models for flow in conduits.

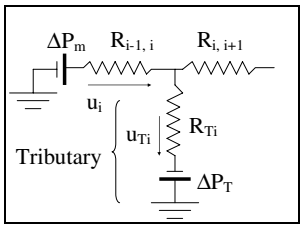

Figure 6. Equivalent system model for filling.